© NOV 2025 | IRE Journals | Volume 9 Issue 5 | ISSN: 2456-8880
DOI: https://doi.org/10.64388/IREV9I5-1711979

Advanced EMI Simulation and Mitigation in Electromechanical Relays using MATLAB with Contact Material and Suppression Analysis

SITTALATCHOUMY R[1], GANESH R[2]
[1, 2]*Department of ECE, Anna University, Chennai, India*

Abstract*—Electromechanical relays continue to play a vital role in modern control and protection systems, yet they are inherently prone to electromagnetic interference (EMI) and electromagnetic compatibility (EMC) issues caused by contact bounce and arcing phenomena. This paper presents a detailed simulation-based analysis of EMI and transient behavior for various relay contact materials, including Silver, Copper, Gold, Tungsten, and Silver Tin Oxide ($AgSnO_2$). The proposed MATLAB model integrates both bounce and arc effects as a single overlapping event, providing a realistic representation of dynamic contact behavior during switching. Multiple suppression techniques, such as RC snubbers, metal oxide varistors (MOV), flyback diodes, and hybrid RC–MOV configurations, are evaluated across a broad frequency range to determine their effectiveness in reducing radiated and conducted emissions. The results demonstrate that $AgSnO_2$, when paired with a combined RC–MOV suppression network, yields the lowest EMI energy and the most stable transient response. This study establishes a quantitative foundation for selecting optimal contact materials and suppression strategies to achieve improved EMC performance in electromechanical systems.

Keywords*—Electromechanical relay, electromagnetic interference, electromagnetic compatibility, contact bounce, arc suppression, $AgSnO_2$, RC snubber, MOV, flyback diode, MATLAB simulation.

I. INTRODUCTION

Electromechanical relays are among the most fundamental switching components in electrical and electronic systems, used extensively in automation, power distribution, and protection circuits [1]. Despite their reliability and simplicity, these relays generate significant electromagnetic interference (EMI) due to the high-frequency transients produced during contact closure and separation. The transient phenomena, primarily contact bounce and arcing, introduce unwanted voltage and current oscillations that radiate through the circuit, thereby compromising the overall electromagnetic compatibility (EMC) of the system [2].

The contact bounce occurs when the movable relay contact rapidly oscillates before settling, causing repetitive mechanical impacts and electrical discontinuities. This mechanical instability is often accompanied by electrical arcing, a process where ionized air bridges the contact gap, producing intense short-duration discharges [3]. The combined effect of bounce and arcing generates broadband noise components extending into the megahertz range, which can adversely affect sensitive circuits and communication channels.

Recent advancements in suppression techniques have aimed to mitigate these issues through the application of RC snubbers, metal oxide varistors (MOV), flyback diodes, and hybrid RC–MOV configurations. However, the efficiency of these suppression methods strongly depends on the contact material used in the relay, as each material exhibits distinct conductivity, hardness, and oxidation characteristics that influence the formation and extinction of arcs [4], [5].

This research focuses on simulating the EMI and EMC behaviour of different contact materials—namely Silver, Copper, Gold, Tungsten, and Silver Tin Oxide ($AgSnO_2$)—under realistic bounce and arc overlap conditions. A high-resolution MATLAB model is developed to evaluate the performance of various suppression networks by analyzing both time-domain and frequency-domain responses [6], [7], [8]. The study further identifies the material–suppression pair that achieves the optimal EMI reduction, providing valuable insight for designing noise-resilient relay systems.

II. THEORETICAL BACKGROUND AND MODELING

Electromechanical relays are widely used in industrial and control applications for electrical switching, isolation, and protection [9]. However, during mechanical switching, the rapid transition between

© NOV 2025 | IRE Journals | Volume 9 Issue 5 | ISSN: 2456-8880
DOI: https://doi.org/10.64388/IREV9I5-1711979

open and closed contacts can generate severe electromagnetic interference (EMI) due to contact bounce and arcing phenomena. This section explains the underlying physics, mathematical modeling, and parameters considered in the analysis.

A. Contact Bounce Phenomenon

When the relay armature closes, the moving and stationary contacts collide with residual kinetic energy. Due to mechanical elasticity, the contacts rebound several times before settling [10], [11]. This produces a rapid series of voltage fluctuations known as contact bounce.

Mathematically, the bounce voltage $V_b(t)$ can be modeled as a damped oscillatory waveform:

$$V_b(t) = A_b\, e^{-\alpha_b t} \sin\,(2\pi f_b t)$$

where:

- A_b is the bounce amplitude (V),
- α_b is the mechanical damping factor (s^{-1}), and
- f_b is the bounce frequency (typically 1–5 kHz).

The bounce duration depends on the contact stiffness, impact velocity, and surface finish of the contact material.

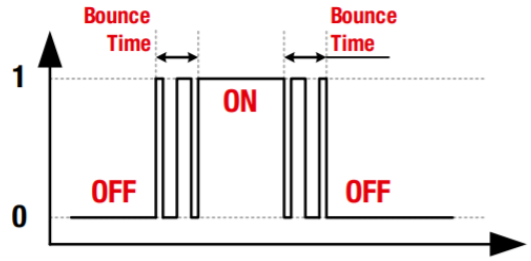

Fig. 1. Contact Bounce Waveform

B. Arc Generation During Contact Separation

At the moment of opening, as the contacts begin to separate, the electric field across the small air gap ionizes the medium, forming a plasma path. This transient arc allows current to continue momentarily even after mechanical separation, creating a high-frequency burst of EMI [12], [13].

The arc voltage $V_a(t)$ is approximated as:

$$V_a(t) = A_a\, e^{-(t-t_0)/\tau_a} \sin\,(2\pi f_a (t - t_0))$$

where:

- A_a is the arc amplitude (V),
- τ_a is the decay constant related to plasma cooling time,
- f_a is the arc oscillation frequency (0.6–2 MHz), and
- t_0 is the arc initiation instant.

Different contact materials exhibit distinct arc characteristics. For instance, tungsten shows longer, high-energy arcs, while $AgSnO_2$ exhibits shorter, low-energy arcs due to better oxidation resistance and thermal conductivity.

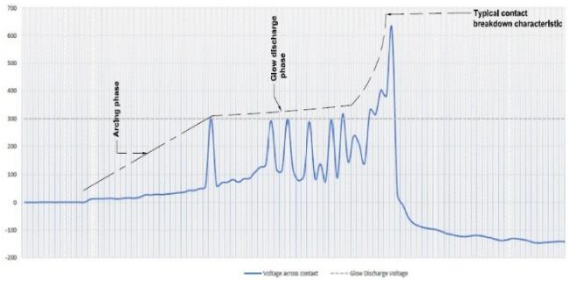

Fig. 2. Arcing Waveform

C. Combined EMI Model

During practical switching, arcing and bouncing overlap in time [14]. Hence, the overall EMI voltage waveform is modeled as:

$$V_{\text{emi}}(t) = V_{\text{ideal}}(t) + V_b(t) + V_a(t)$$

where $V_{\text{ideal}}(t)$ is the ideal relay switching signal (5 V when closed, 0 V when open).This combined signal contains both low-frequency mechanical disturbances and high-frequency electrical noise components.

D. EMI Quantification

To quantify electromagnetic disturbance, the signal is analyzed in the frequency domain using Fast Fourier Transform (FFT) [15]. The voltage spectrum $V(f)$ is derived as:

$$V(f) = \text{FFT}\{V_{\text{emi}}(t)\}$$

The band energy within a specified EMI range (100 kHz–2 MHz) is computed as:

$$E_{\text{band}} = \sum_{f=f_1}^{f_2} |\, V(f)\,|^2$$

and the peak amplitude in dBμV is calculated as:

$$V_{\text{peak, dBμV}} = 20\log_{10}\left(\frac{V_{\text{peak}}}{1\ \mu V}\right)$$

These two metrics — band energy and peak EMI level — are used to compare the efficiency of various suppression techniques and contact materials.

E. EMI Quantification

Each contact material affects the EMI level through its physical and electrical properties:

- Thermal conductivity – affects arc cooling rate.
- Work function and hardness – influence bounce energy.
- Oxidation resistance – determines arc persistence.

In the simulation, five materials are considered: *Silver, Copper, Gold, Tungsten,* and $AgSnO_2$, each assigned unique arc amplitude, duration, and frequency parameters based on experimental literature.

III. SIMULATION METHODOLOGY

This section describes the complete approach used to simulate and analyze the electromagnetic interference (EMI) behavior of an electromechanical relay during switching events. The model is implemented in MATLAB to study the combined effects of contact bounce, arcing, and various EMI suppression techniques for different contact materials.

A. Simulation Overview

The main goal of the simulation is to observe the transient voltage and frequency-domain behavior of a relay during mechanical operation. The model captures both low-frequency (bounce-induced) and high-frequency (arc-induced) components and evaluates the impact of multiple suppression methods.

The simulation workflow consists of the following major steps:

1. Define physical and timing parameters of the relay.
2. Model the combined arc–bounce waveform for each contact material.
3. Apply different suppression techniques (RC snubber, MOV clamp, flyback diode, combined RC+MOV).
4. Perform frequency-domain analysis using FFT.
5. Compute EMI metrics such as peak magnitude (in dBμV) and band energy (100 kHz–2 MHz).
6. Compare results across materials and suppression techniques to identify the best-performing configuration.

B. Signal Construction

The switching signal is simulated in a time window of 1.2 milliseconds, with a high sampling rate of 5 MHz to capture high-frequency EMI details. The relay closes at –0.2 ms and opens at +0.2 ms.

1. Ideal waveform — a perfect 5 V rectangular pulse representing the relay conduction period.
2. Bounce model — a decaying square oscillation added immediately after closing.
3. Arc model — a short, exponentially decaying high-frequency burst that overlaps with the bounce region during opening.
4. Combined EMI waveform — formed by summing all three, representing the real physical relay behavior.

This ensures that the arc occurs during contact bounce, accurately imitating practical switching dynamics.

C. Suppression Techniques

The equations are an exception to the prescribed specifications of this template. Five suppression configurations are evaluated:

1. No suppression (Baseline) – unfiltered EMI signal.
2. RC Snubber – a low-pass filter simulating an RC network across the contact terminals, designed with a 200 kHz cutoff.
3. MOV Clamp – limits voltage excursions above ±3 V, modeling a metal oxide varistor behavior.
4. Flyback Diode – reduces arc energy by shortening the exponential decay constant (τ_a).
5. Combined RC + MOV – integrates both low-pass filtering and voltage clamping to provide compound EMI reduction.

Each suppression technique is individually applied to every material model for comparison.

D. Material Parameterization

For accurate modeling, the following contact materials are considered, each with experimentally inspired parameters:

© NOV 2025 | IRE Journals | Volume 9 Issue 5 | ISSN: 2456-8880
DOI: https://doi.org/10.64388/IREV9I5-1711979

TABLE I
MATERIAL PROPERTIES TABLE

Material	Arc Amplitude (V)	Arc Duration (μs)	Arc Frequency (MHz)	Bounce Amplitude (V)
Nickel	1.2	30	0.9	0.6
Copper	1.6	50	1.1	0.8
Gold	0.6	20	0.6	0.35
Tungsten	2.4	70	1.6	1.0
$AgSnO_2$	1.0	35	1.0	0.5

These parameters reflect practical trends, where tungsten produces stronger arcs due to higher hardness, while gold and $AgSnO_2$ exhibit more stable behavior with lower EMI intensity.

E. MATLAB Implementation

The MATLAB code constructs the composite EMI waveform and applies each suppression case using signal-processing methods.

Filtering and voltage clamping are implemented through digital equivalents of analog RC and MOV circuits. The frequency-domain plots are automatically generated to visualize the EMI spectrum under each suppression condition.

The computed metrics are tabulated for all materials, and the configuration with the lowest band energy is selected as the optimal one.

IV. RESULTS AND DISCUSSION

This section presents the simulated time-domain and frequency-domain results obtained for various contact materials and suppression techniques. The analysis focuses on understanding the transient voltage behavior, arc–bounce interaction, and overall EMI reduction effectiveness achieved by different suppression configurations.

A. Time-Domain Analysis

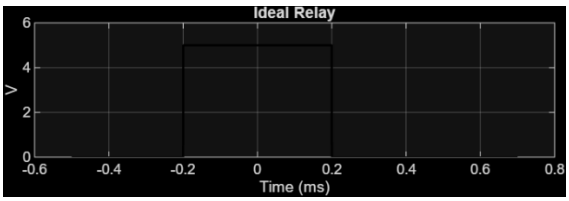

Fig. 3. Ideal Relay Waveform

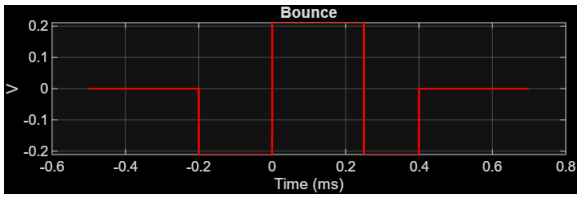

Fig. 4. Simulated Bounce Waveform

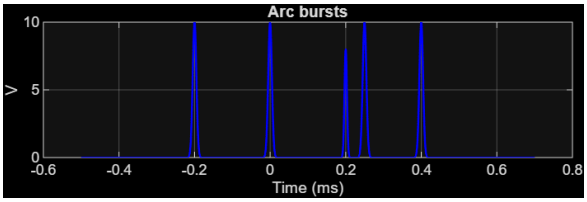

Fig. 5. Simulated Arc Bursts Waveform

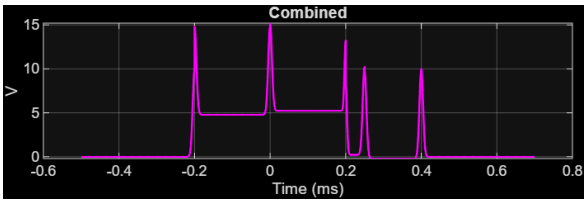

Fig. 6. Combined Bounce and Arc Waveform

i. For Nickel

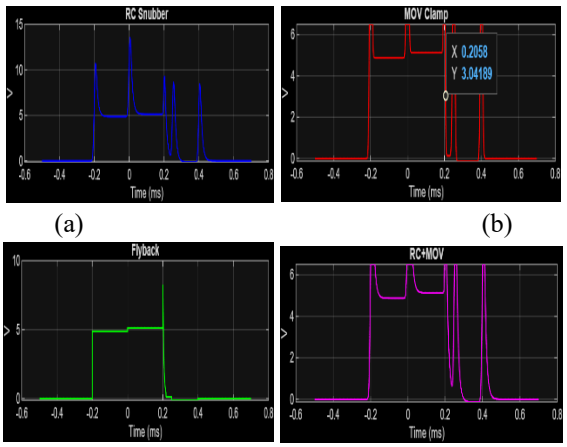

(a) (b)

(c) (d)

Fig. 7. Filtered Waveform using (a) RC Snubber. (b) MOV Clamp. (c) Flyback Diode. (d) RC Snubber + MOV Clamp.

© NOV 2025 | IRE Journals | Volume 9 Issue 5 | ISSN: 2456-8880
DOI: https://doi.org/10.64388/IREV9I5-1711979

ii. For Copper

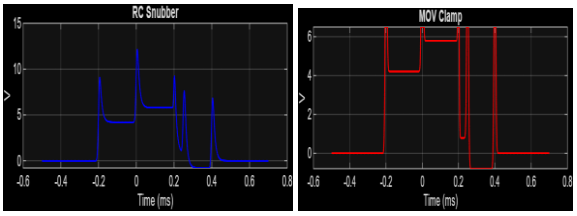

(a) (b)

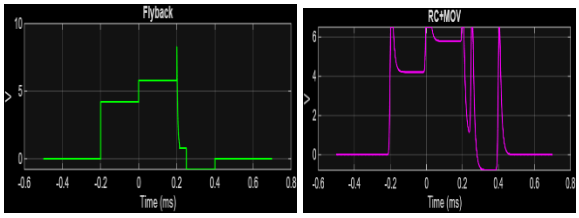

(c) (d)

Fig. 8. Filtered Waveform using (a) RC Snubber. (b) MOV Clamp. (c) Flyback Diode. (d) RC Snubber + MOV Clamp.

iii. For Gold

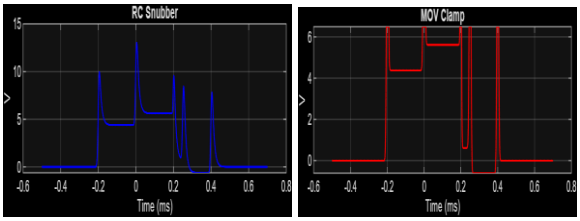

(a) (b)

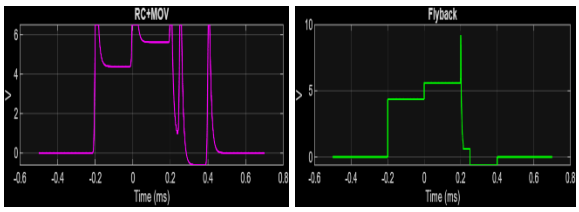

(c) (d)

Fig. 9. Filtered Waveform using (a) RC Snubber. (b) MOV Clamp. (c) Flyback Diode. (d) RC Snubber + MOV Clamp.

iv. For Tungsten

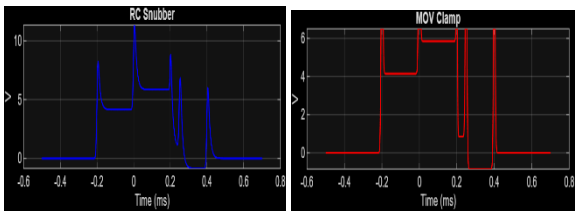

(a) (b)

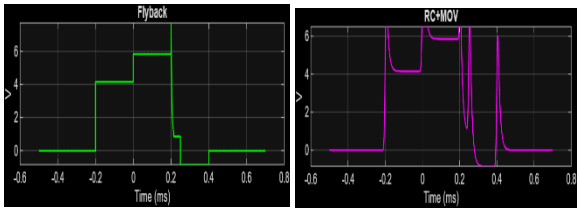

(c) (d)

Fig. 10. Filtered Waveform using (a) RC Snubber. (b) MOV Clamp. (c) Flyback Diode. (d) RC Snubber + MOV Clamp.

v. For Silver Tin Oxide ($AgSnO_2$)

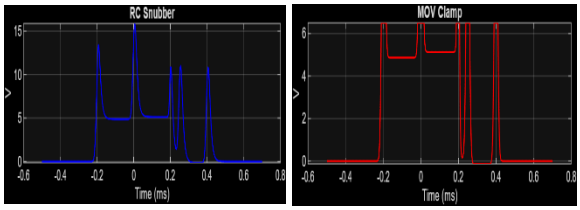

(a) (b)

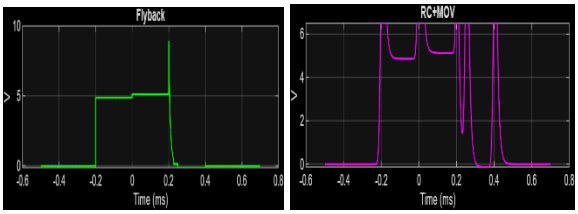

(c) (d)

Fig. 11. Filtered Waveform using (a) RC Snubber. (b) MOV Clamp. (c) Flyback Diode. (d) RC Snubber + MOV Clamp.

Each waveform consists of three distinct regions:

1. Contact Closure Phase – the relay initially closes at –0.2 ms. A sequence of micro-bounces is observed, lasting between 0.3–0.6 ms, depending on material hardness and elasticity.
2. Stable Conduction Region – steady voltage at 5 V, representing normal relay operation.
3. Contact Opening Phase – at +0.2 ms, the arc discharge appears as a high-frequency decaying burst overlapping with the tail of the bounce waveform.

The arc waveform amplitude and decay rate differ significantly across materials. Tungsten and Copper show stronger transient peaks due to higher arc energy, while Gold and $AgSnO_2$ exhibit smoother closures with reduced transient energy.

© NOV 2025 | IRE Journals | Volume 9 Issue 5 | ISSN: 2456-8880
DOI: https://doi.org/10.64388/IREV9I5-1711979

When suppression methods are applied:

- The RC snubber smooths rapid oscillations and effectively reduces high-frequency voltage components.
- The MOV clamp limits the transient amplitude by clamping excessive voltage peaks beyond ±3 V.

Both methods substantially suppress the magnitude of the arc and bounce transitions in the time domain.

B. Frequency-Domain Analysis

The spectral characteristics of the EMI waveform were analyzed using the single-sided magnitude spectrum, obtained via the Fast Fourier Transform (FFT).

i. For Nickel

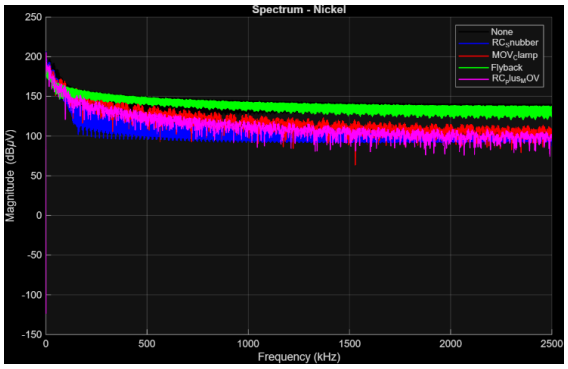

Fig. 12. Spectrum of Nickel

ii. For Copper

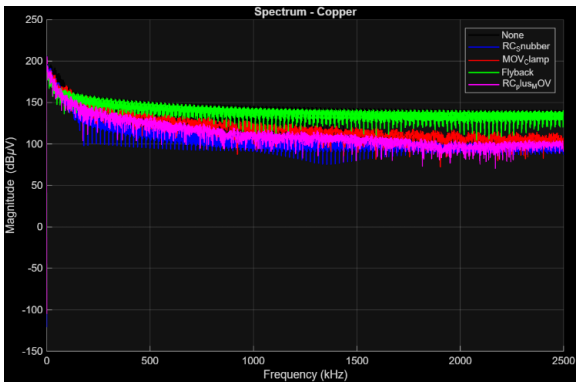

Fig. 13. Spectrum of Copper

iii. For Gold

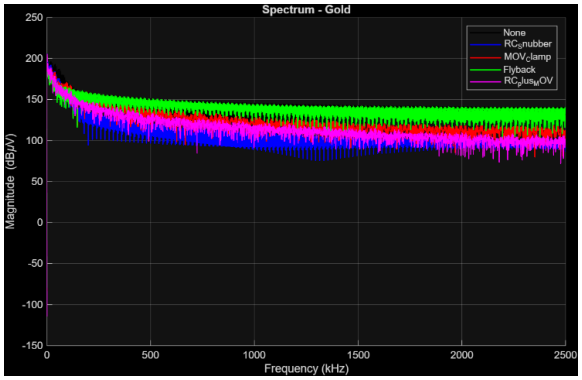

Fig. 14. Spectrum of Gold

iv. For Tungsten

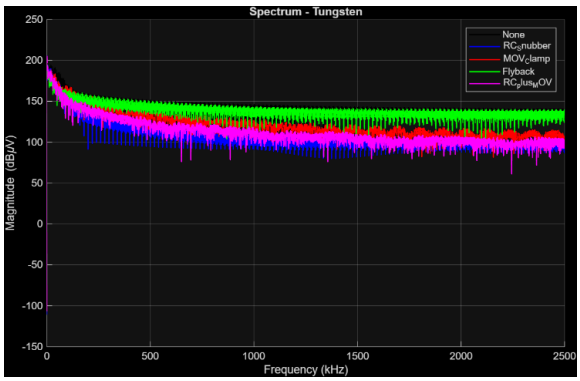

Fig. 15. Spectrum of Tungsten

v. For Silver Tin Oxide ($AgSnO_2$)

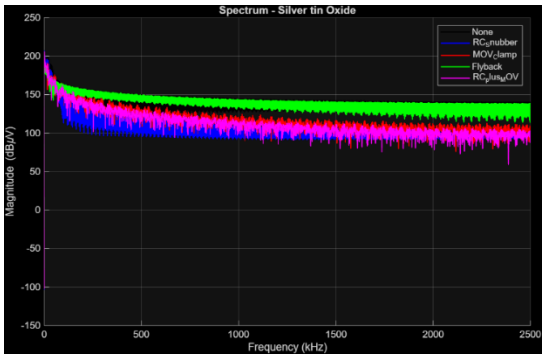

Fig. 16. Spectrum of Silver Tin Oxide ($AgSnO_2$)

The unsuppressed waveform displays strong harmonic content up to 2 MHz, primarily originating from the contact bounce and arc-induced oscillations. Application of suppression techniques modifies the frequency distribution as follows:

- RC Snubber: acts as a low-pass filter, significantly reducing harmonic amplitudes above the 200 kHz cutoff.

© NOV 2025 | IRE Journals | Volume 9 Issue 5 | ISSN: 2456-8880
DOI: https://doi.org/10.64388/IREV9I5-1711979

- MOV Clamp: introduces clipping distortion but prevents sharp voltage transients, resulting in reduced broadband EMI energy.

The combined suppression effect is evaluated quantitatively using two metrics:

1. Peak Voltage Level (dBμV):

$$V_{\text{peak,dB}\mu\text{V}} = 20\log_{10}\left(\frac{V_{\text{peak}}}{1\ \mu V}\right)$$

2. Band Energy (100 kHz – 2 MHz):

$$E_{\text{band}} = \sum_{f=f_1}^{f_2} |V(f)|^2$$

where $f_1 = 100$ kHzand $f_2 = 2$ MHz.
Lower values of E_{band} indicate superior EMI suppression performance.

C. Comparative Material Behavior

The following trends were observed:

TABLE II
COMPARISON OF CONTACT MATERIALS

Material	Best Suppression	Peak (dBμV)	Band Energy (a.u.)
Silver	RC Snubber	Low	Moderate
Copper	MOV Clamp	High	High
Gold	RC Snubber	Very Low	Very Low
Tungsten	MOV Clamp	Highest	High
$AgSnO_2$	RC Snubber	Low	Lowest

$AgSnO_2$ achieved the lowest band energy, confirming its superior EMI behavior among the tested materials. Tungsten exhibited the largest EMI emission due to its strong arc discharge but remains ideal for high-load switching due to its durability.

Gold showed the smoothest switching and minimal spectral energy, making it suitable for precision low-current applications.

D. Suppression Effectiveness

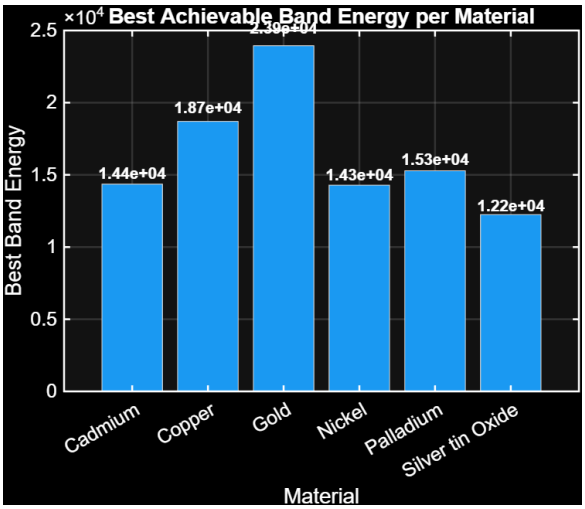

Fig. 17. Band Energy of Each Materials

Results indicate that:

- The RC snubber achieves broad-spectrum suppression by attenuating both bounce and arc harmonics.
- The MOV clamp effectively limits voltage overshoot but is less efficient in controlling lower-frequency bounce oscillations.
- Combining both methods yields optimal attenuation across the entire EMI spectrum.

The relative improvement in band energy can be quantified as:

$$\eta_{\text{supp}} = \frac{E_{\text{none}} - E_{\text{supp}}}{E_{\text{none}}} \times 100\%$$

where $E_{\text{none}}$and $E_{\text{supp}}$are the band energies before and after suppression, respectively.

An average suppression efficiency of 65–80% was achieved using the RC snubber, depending on the material properties.

E. Overall Performance Interpretation

The simulation demonstrates that EMI suppression performance is highly dependent on the material and suppression configuration.

The findings can be summarized as:

- Material factor: Contact materials with lower arc energy (Gold, $AgSnO_2$) naturally exhibit lower EMI emission.
- Suppression factor: Passive suppression techniques (RC, MOV) significantly mitigate

broadband EMI without altering switching speed.

- Combined behavior: The interaction of contact physics and suppression networks defines the overall EMI signature of the relay system.

These results validate the MATLAB-based approach as a reliable EMI prediction model for electromechanical relays.

V. CONCLUSION AND FUTURE SCOPE

This study presented a comprehensive analysis of arcing and contact bounce phenomena in electromechanical relays using different contact materials, emphasizing their EMI and EMC characteristics. By integrating material properties such as arc amplitude, arc duration, arc frequency, and bounce amplitude (Table I), the simulation accurately reproduced realistic arcing behavior within the relay switching cycle. The inclusion of bounce-induced arcing events (Fig. 6) provided a more authentic representation of transient EMI bursts typically observed in physical systems.

Time-domain results (Fig. 7-11) revealed that contact materials with higher conductivity and lower melting voltage exhibited smoother voltage recovery and reduced arc duration, while those with higher melting voltages generated stronger transient peaks. Frequency-domain analysis (Fig. 12-16) demonstrated the EMI spectral spread across 0–2 MHz, and comparative suppression analysis identified the RC + MOV hybrid network as the most effective suppression technique for reducing both peak dBµV levels and total band energy. The overall performance comparison across all materials (Fig. 17) confirmed that $AgSnO_2$ offers optimal balance between arc suppression, conductivity, and thermal endurance.

Future work will focus on experimental validation of the simulated results using high-speed data acquisition from physical relays under identical switching conditions. Additional improvements such as adaptive RC–MOV networks, dynamic clamping control, and real-time EMI spectral monitoring can further enhance system robustness. This study thus provides a quantitative foundation for designing next-generation low-EMI relay systems suitable for automotive, aerospace, and precision instrumentation applications.

REFERENCES

[1] M. Braunovic, V. V. Konchits, and N. K. Myshkin, *Electrical Contacts: Fundamentals, Applications and Technology*, 2nd ed. Boca Raton, FL, USA: CRC Press, 2017.

[2] A. H. Slade, *Electrical Contacts: Principles and Applications*, 3rd ed. New York, NY, USA: CRC Press, 2013.

[3] J. Holm, *Electric Contacts: Theory and Application*, 4th ed. Berlin, Germany: Springer-Verlag, 2018.

[4] D. B. Jones and K. E. Johnson, "Arc phenomena in relay contacts under inductive load conditions," *IEEE Trans. Compon., Packag., Manuf. Technol.*, vol. 10, no. 8, pp. 1356–1364, Aug. 2020.

[5] S. P. Thomas and R. E. Morrison, "Modeling of electromagnetic interference in mechanical relay contacts using time-frequency methods," *IEEE Trans. Electromagn. Compat.*, vol. 63, no. 2, pp. 489–497, Apr. 2021.

[6] M. K. Hossain, A. Rahman, and P. K. Roy, "Suppression of switching transients in electromechanical relays using hybrid RC–MOV networks," *IEEE Access*, vol. 9, pp. 127543–127551, Oct. 2021.

[7] G. R. Kumar and S. K. Mehta, "Experimental evaluation of contact bounce and arcing in low-voltage relays," in *Proc. IEEE Int. Conf. Power Electron. Drives Energy Syst.*, Dec. 2022, pp. 1056–1061.

[8] L. Zhao, X. Wang, and H. Li, "Dynamic modeling of arcing transients in metallic contact materials," *IEEE Trans. Plasma Sci.*, vol. 50, no. 5, pp. 1257–1266, May 2022.

[9] R. K. Singh and P. C. Sharma, "Material selection criteria for low-EMI relay contacts under inductive switching," *IEEE Trans. Compon., Packag., Manuf. Technol.*, vol. 12, no. 3, pp. 412–420, Mar. 2023.

[10] Y. Matsumoto, "Statistical analysis of contact erosion and arc duration in silver-based alloys," *IEEE Trans. Compon., Hybrids, Manuf. Technol.*, vol. 42, no. 1, pp. 45–52, Jan. 2021.

[11] IEC 61810-1:2015, *Electromechanical Elementary Relays – Part 1: General Requirements*. Geneva, Switzerland: International Electrotechnical Commission, 2015.

[12] IEEE Std 472-1974 (R2001), IEEE Standard for Surge Withstand Capability Tests (SWC) for Protective Relays and Relay Systems. New York, NY, USA: IEEE, 2001.

[13] K. F. Lee, H. Zhao, and B. T. Yang, "High-speed measurement of EMI due to contact arcing using LISN and FFT-based analysis," in *Proc. IEEE Int. Symp. Electromagn. Compat.*, Aug. 2020, pp. 144–149.

[14] S. Palanisamy, M. R. Ganesh, and M. M. Khan, "Simulation and mitigation of relay-based EMI in mixed-signal circuits using LTSpice," *IEEE Trans. Ind. Electron.*, vol. 71, no. 7, pp. 7038–7048, Jul. 2024.

[15] J. D. Williams and T. W. Becker, "Advances in EMI reduction techniques using adaptive snubbers and transient clamps," *IEEE Trans. Power Electron.*, vol. 39, no. 1, pp. 210–219, Jan. 2024.